Near-field-induced optical force on a metal particle and C_{60}: Real-time and real-space electron dynamics simulation

Takeshi Iwasa[1] and Katsuyuki Nobusada[1,2,*]

[1]*Department of Theoretical and Computational Molecular Science, Institute for Molecular Science, Myodaiji, Okazaki 444-8585, Japan*

[2]*Department of Structural Molecular Science, School of Physical Sciences, The Graduate University for Advanced Studies, Myodaiji, Okazaki 444-8585, Japan*

(Received 19 May 2010; published 8 October 2010)

Optical forces induced by a near field are calculated for a 1-mm-sized metal particle mimicked by a jellium model and for C_{60} in the framework of real-time and real-space time-dependent density-functional theory combined with a nonuniform light-matter interaction formalism, fully taking account of multipole interaction. A highly localized near field nonuniformly polarizes these molecules. The locally induced polarization charges in the molecules are partly canceled by the screening charges. The polarization and screening charges generally contribute to the attractive and repulsive forces, respectively, and a sensible balance between these charges results in several peaks in the optical force as a function of the frequency of the near field. The resonance excitation does not necessarily maximally induce the net force, and the force exerted on the molecules strongly depends on the details of their electronic structures. The optical force is larger in the metal particle than in C_{60}. We also found that the optical force depends linearly on the intensity of the near field.

DOI: 10.1103/PhysRevA.82.043411 PACS number(s): 37.10.Pq, 31.15.E−, 31.50.Df, 33.80.−b

I. INTRODUCTION

Optical trapping of micrometer-sized particles by lasers was reported in the pioneering work by Ashkin [1], and this idea was eventually realized as an innovative tool: a single-beam gradient-force optical trap for dielectric particles, called "optical tweezers" [2]. In a series of papers since this seminal work, Ashkin and co-workers have succeeded in optically trapping and manipulating various types of objects [3]. The optical tweezers, using force exerted by a highly focused laser beam, can trap and manipulate objects, now in practice ranging in force up to 100–200 pN with subpiconewton resolution and in size from tens of nanometers to tens of micrometers. Such laser-based optical traps have been used in a wide range of applications [4,5] to atoms and small molecules [3], colloidal particles [6,7], and biological objects [8–10]. In particular, biological applications have been extensively used to study mechanical or functional properties of cells, intercellular materials, and filaments and also to study biological motors. A large number of references of those biological applications were compiled in the resource letters [11].

Although a complete description of the laser-based optical traps needs a fully quantum mechanical treatment, the optical force exerted on trapped objects can be derived from the Maxwell stress tensor into two limiting cases where the size of the object is much larger (i.e., infinitely extended systems) and much smaller (i.e., small particle systems) than the wavelength of an incident laser field [12]. In the limiting case of extended systems, the net force is associated with so-called optical pressure. In the other limiting case of small-particle systems, the net force is considered to be a gradient force. Since in this article we study nanoparticle and light interaction, only the gradient force exerted by the optical field is discussed. The gradient force is expected to be exerted more efficiently by using a near field in optical traps because the near field is a very short-range electromagnetic field with a strong intensity gradient. Such a short-range field has the advantage of improving resolution beyond the diffraction limit. In addition, the near-field enhancement, which is a consequence of self-consistent light-matter interaction, enables the trapping of objects with a weaker incident laser beam. Novotny and co-workers proposed a theoretical scheme for using optical forces by the near field close to a laser-illuminated metal tip [13]. They demonstrated that strong mechanical force and torque were exerted on dielectric particles in aqueous environments at the nanometer scale.

In recent years, laser-based optical phenomena in nanostructures, including the optical traps mentioned previously, have been intensively studied in a rapidly growing research area, referred to as "nano-optics" or "nanophotonics." The fundamental features of those optical phenomena are understood in the more general context of light-matter interaction in optical response theory. A semiclassical approach has so far been employed to understand these phenomena because a fully quantum mechanical treatment, that is, quantum electrodynamics theory, is almost impossible in practice to perform for real nanostructure systems. In the semiclassical approach, an optical field is determined by the Maxwell equation and a material is described quantum mechanically, and the resulting Maxwell and Schrödinger coupled equation should be solved self-consistently [14–16]. However, it is still computationally highly demanding to carry out the coupled equation in real systems [17,18]. Instead of treating the coupled equation rigorously, many authors employed numerically feasible approaches in which, particularly, the target objects were phenomenologically approximated by model materials such as dielectrics to avoid fully solving electronic structure calculations [13,19–23].

Detailed electronic structures of molecules play an essential role in molecular science because they determine all the properties of materials such as geometry, bonding character,

*nobusada@ims.ac.jp

 ©2010 The American Physical Society

stability, functionality, and reactivity. In general, absorption spectra of molecules become discrete with many sharp peaks as the system decreases in size. Each peak is apparently associated with detailed electronic structures consisting of discrete energy levels of molecules. This is because the light-matter interaction in such molecular systems can change drastically depending on the electronic structures. One simple and clear example is the resonance effect in absorption spectra. As is easily inferred from this characteristic, the optical force also strongly depends on details of the electronic structures of nanometer-sized objects. This means that we can optically trap and manipulate an object more precisely by changing the incident laser frequency or the position of the exerted force on an object. For these reasons, it is very important to analyze the optical force on nanostructures, explicitly taking account of the electronic structures of objects.

We recently reported the first-principles electron dynamics simulation approach to solving optical response, fully taking account of nonuniform light and matter interaction [24]. This approach has the following advantages: (i) Electronic structure and electron dynamics calculations are carried out at the level of density-functional theory (DFT) and time-dependent (TD) DFT, respectively. (ii) Full nonuniform light and matter interactions (i.e., full-multipole effects) are included. (iii) Electron dynamics simulation in real space and real time makes it much easier to analyze and visualize the optical response of a target molecule. In the present study, we employ this approach to understand the mechanisms of the optical force exerted on nanostructures interacting with a near field. Special emphasis is placed on elucidating the effect of the detailed molecular-electronic structures on the optical force.

The article is organized as follows. In the next section, we briefly review the light-matter interaction formalism combined into the real-time and real-space TDDFT approach. The model system and computational details are described in Sec. III. The results and the concluding remarks are given in Secs. IV and V, respectively.

II. THEORY

We first briefly review the nonuniform light-matter interaction approach developed in our previous study [24]. An interaction Hamiltonian $\hat{H}_{\rm int}$ fully including the spatial variation of an electric field can be derived from the multipolar Hamiltonian without magnetic interactions as follows [25]:

$$\hat{H}_{\rm int}(t) = -\int d\boldsymbol{r}\,\hat{\boldsymbol{P}}(\boldsymbol{r})\cdot\boldsymbol{E}(\boldsymbol{r},t), \tag{1}$$

where $\hat{\boldsymbol{P}}$ is the polarization of a molecule and $\boldsymbol{E}$ is an electric field. We use the exact form of a polarization operator acting on electrons in a molecule [26,27] as follows:

$$\hat{\boldsymbol{P}} = -\sum_i(\hat{\boldsymbol{q}}_i - \boldsymbol{R})\int_0^1 d\lambda\,\delta(\boldsymbol{r} - \boldsymbol{R} - \lambda(\hat{\boldsymbol{q}}_i - \boldsymbol{R})), \tag{2}$$

where $\hat{\boldsymbol{q}}_i$ is the position operator of the ith electron in a molecule and $\boldsymbol{R}$ is the center of mass coordinate of a molecule. The expectation value of the interaction Hamiltonian is written in the form of

$$\langle\hat{H}_{\rm int}\rangle = \int d\boldsymbol{r}\,\rho(\boldsymbol{r},t)\,(\boldsymbol{r} - \boldsymbol{R})\cdot\int_0^1 d\lambda\boldsymbol{E}(\boldsymbol{R} + \lambda(\boldsymbol{r} - \boldsymbol{R}),t), \tag{3}$$

where ρ is the electron density. We define the effective electric field and the effective potential by

$$\boldsymbol{E}_{\rm eff}(\boldsymbol{r},t) \equiv \int_0^1 d\lambda\boldsymbol{E}(\boldsymbol{R} + \lambda(\boldsymbol{r} - \boldsymbol{R}),t), \tag{4}$$

$$V_{\rm eff}(\boldsymbol{r},t) \equiv (\boldsymbol{r} - \boldsymbol{R})\cdot\boldsymbol{E}_{\rm eff}(\boldsymbol{r},t). \tag{5}$$

The effective potential $V_{\rm eff}$ is incorporated into the time-dependent Kohn-Sham (TDKS) equation [28,29]:

$$i\hbar\frac{\partial}{\partial t}\psi_j(\boldsymbol{r},t) = \left[-\frac{\hbar^2}{2m}\nabla^2 + V_{\rm KS}[\rho](\boldsymbol{r},t)\right]\psi_j(\boldsymbol{r},t), \tag{6}$$

where m is the electron mass and ψ_j is the KS wave function relating to the electron density by

$$\rho(\boldsymbol{r},t) = 2\sum_{j=1}^{N/2}|\psi_j(\boldsymbol{r},t)|^2. \tag{7}$$

The KS potential $V_{\rm KS}[\rho](\boldsymbol{r},t)$ consists of four terms of an ion-electron interaction potential $V_{\rm ion}(\boldsymbol{r})$, a time-dependent Hartree potential, an exchange-correlation potential $V_{\rm xc}[\rho](\boldsymbol{r},t)$, and an external potential $V_{\rm eff}$ as follows:

$$V_{\rm KS}[\rho](\boldsymbol{r},t) = V_{\rm ion}(\boldsymbol{r}) + \frac{1}{4\pi\varepsilon_0}\int\frac{\rho(\mathbf{r}',t)}{|\boldsymbol{r} - \boldsymbol{r}'|}d\mathbf{r}' + V_{\rm xc}[\rho](\boldsymbol{r},t) + V_{\rm eff}(\boldsymbol{r},t). \tag{8}$$

We do not consider the damping effect due to electron-nuclear coupling or thermal relaxation on the electron dynamics. Thus, the response of the molecule could be artificially strong in the present model. Ideally, it is necessary to treat the electron dynamics in the presence of such relaxation, although it is practically almost impossible in real nanostructure systems. In an effort to accurately describe the optical force exerted on molecules at the level of molecular theory, we here carry out the first-principles calculations of electron dynamics as a first step and leave the relaxation effect for future investigation.

The optical force exerted on the center of mass of a nanoparticle in the time domain can be written in the form of

$$\boldsymbol{F}(t) = -\int[\rho(\boldsymbol{r},t) - \rho(\boldsymbol{r},0)]\boldsymbol{E}(\boldsymbol{r},t)\,d\boldsymbol{r}. \tag{9}$$

It should be noted that $\rho(\boldsymbol{r},t) - \rho(\boldsymbol{r},0)$ is the net or true induced charge distribution and numerically includes the full contributions of the charges screening the external electric field within the molecule, that is, an internal electric field effect. To obtain the net force, the time average of this quantity over the pulse duration T is taken:

$$\langle\boldsymbol{F}\rangle = \frac{1}{T}\int_0^T\boldsymbol{F}(t)\,dt. \tag{10}$$

If a target material has a complex structure unlike a sphere used in this article, it might be useful to define local optical forces acting on each local structure of a material.

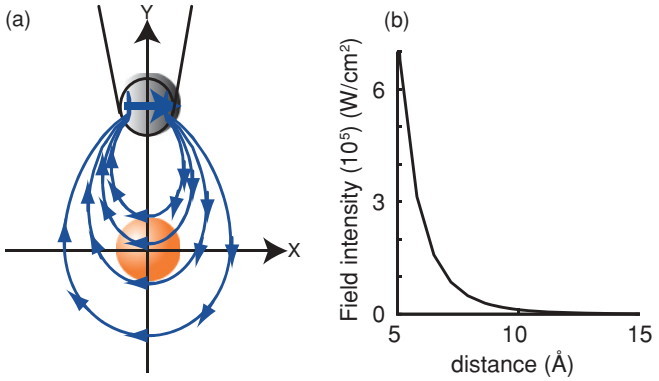

FIG. 1. (Color online) (a) Schematic of a near-field fiber tip (gray ball) and a target particle (orange ball). The near field is approximated by the radiation from an x-polarized oscillating dipole (solid blue arrow). The blue curves denote the electric field lines. (b) Electric field intensity as a function of distance between the tip and the particle.

III. MODEL SYSTEM AND COMPUTATIONAL DETAILS

We consider that a nanoparticle interacts with the near field radiated from an x-polarized oscillating dipole at 10 Å above the molecule center, $(x,y,z) = (0,0,0)$, as shown in Fig. 1(a). The spatial distribution of the near field is given by [30]

$$\boldsymbol{E}(\boldsymbol{r} - \boldsymbol{R}_{\rm dip}) = \frac{[3\boldsymbol{n}(\boldsymbol{n}\cdot\boldsymbol{\mu}) - \boldsymbol{\mu}]}{(4\pi\varepsilon_0|\boldsymbol{r} - \boldsymbol{R}_{\rm dip}|)^3} e^{i\boldsymbol{k}\cdot(\boldsymbol{r}-\boldsymbol{R}_{\rm dip})}, \qquad (11)$$

where $\boldsymbol{R}_{\rm dip}$ is the coordinate of the oscillating dipole, k is the wave number, ε_0 is the vacuum permittivity, $\boldsymbol{n}$ is the unit vector of $(\boldsymbol{r} - \boldsymbol{R}_{\rm dip})/|\boldsymbol{r} - \boldsymbol{R}_{\rm dip}|$, and $\boldsymbol{\mu}$ is the dipole moment of the radiation source. We set $\boldsymbol{R}_{\rm dip} = (0.0, 10.0, 0.0)$ Å and $\boldsymbol{\mu} = (0.01, 0.0, 0.0)$ D. As shown in Fig. 1(b), the intensities of the near field are 7.6×10^5, 1.2×10^4, and 1.0×10^3 W/cm^2 at $(x,y) = (0.0, 5.0)$, $(0.0, 0.0)$, and $(0.0, -5.0)$ Å, respectively. The external potential $V_{\rm eff}$ is calculated by Eq. (5) with the effective electric field Eq. (4) where the electric field $\boldsymbol{E}$ is given by the dipole radiation, Eq. (11). We set the center of mass of the molecule to be the origin. The temporal shape of the near field is taken as a pulse. Finally, the effective potential Eq. (5) is rewritten by

$$V_{\rm eff}(\boldsymbol{r},t) = -\boldsymbol{r}\cdot\boldsymbol{E}_{\rm eff}(\boldsymbol{r})\sin(\omega t)\sin^2\left(\frac{\pi t}{T}\right) \quad (0 < t < T), \qquad (12)$$

where ω is the frequency of the oscillating dipole and T determines the pulse duration.

We demonstrate the TDDFT simulation of the optical force in different two systems: a metal nanoparticle and C_{60}. The metal nanoparticle is simplified by a jellium model, in which the ionic background is given by

$$V_{\rm ion}(\boldsymbol{r}) = \frac{3}{4\pi r_s^3}\left[1 + \exp\left(\frac{|\boldsymbol{r}| - a}{w}\right)\right]^{-1}, \qquad (13)$$

where r_s is the density parameter [31], a is the radius of the sphere, and w is the smoothed-out factor for the jellium surface. The jellium parameters for the metal nanoparticle are set to $r_s = 1.60$ (i.e., this value corresponds to bulk silver and then the total number of electrons in the nanoparticle is 34), $a = 0.5$ nm, and $w = 0.538$. For C_{60}, on the other hand, the ionic background $V_{\rm ion}(\boldsymbol{r})$ of an atomic component C is constructed from a norm-conserving pseudopotential generated numerically following the Troullier and Martins procedure [32]. In this article, we use the Kleinman-Bylander separable form to represent the nonlocal (i.e., angular-momentum-depending) potential terms [33]. The C−C distances are set to be 1.457 Å for the single bond and 1.384 Å for the double bond. The inner shell structure of the carbon atom is approximated by an effective core pseudopotential, and then the remaining four electrons ($2s^2 2p^2$) are explicitly treated, that is, 240-electron dynamics simulation in total for C_{60}. To represent the exchange-correlation potential $V_{\rm xc}(\boldsymbol{r},t)$, we use the local density approximation given by Perdew and Zunger [34] as in the previous study.

The TDKS equation, Eq. (6), for these particles is solved numerically by a grid-based method [29,35–41] in a three-dimensional Cartesian-coordinate cubic box. For the metal particle, the length of the cubic box is 26 Å, and uniform grids with a mesh spacing of 0.5 Å are used, while the length and the mesh spacing are 16 Å and 0.3 Å, respectively, for C_{60}. The Laplacian operator is evaluated by a nine-point difference formula [35]. The time propagation of the KS orbitals is carried out with a fourth-order Taylor expansion by using constant time steps of 0.005 fs for the metal particle and 0.002 fs for C_{60}.

The effective potential for the dipole radiation on each grid is computed by combining Eqs. (4), (5), and (11). The integral of Eq. (4) is calculated numerically with a constant spacing of $\Delta\lambda = 0.0423$ Å. In the integration, $\boldsymbol{E}$ is evaluated as $4\pi\boldsymbol{\mu}/3$ if $|\boldsymbol{E}|$ is larger than $|4\pi\boldsymbol{\mu}/3|$, including the position of the dipole [25]. This is done for a few points very close to the dipole, that is, $|\boldsymbol{r} - \boldsymbol{R}_{\rm dip}| \sim 0.2$ Å. The pulse duration ($T = 20$ fs) is short enough to avoid considering the nuclear dynamics, and thus the ion position is fixed during the time evolution.

Before ending this section, we comment on the validity of the theoretical model. We do not consider the self-consistent light-matter interaction between the target molecule and radiation source. More specifically, we employ a theoretical model as in the case of the previous study in which the near field is considered to be a radiation field from an oscillating dipole source and the back reaction of the electric field due to the target molecule on the source field is negligible. However, in the present theoretical model, the size of the target molecule is relatively small, and its induced dipole is not so strong. Thus, it can be reasonably assumed that the back reaction does not primarily affect the external source field. We need to explicitly take account of the back reaction when the target molecule becomes larger and its induced dipole is comparable with the oscillating dipole of the radiation source. The effect of the back reaction might be noticeable especially under the resonant condition and then should be treated by solving the Maxwell-Schrödinger coupled equation in a self-consistent manner. As mentioned in the beginning of this article, it is still computationally highly demanding to solve such a coupled equation in real nanostructure systems. In a model two-particle system, for instance, Yan et al. discussed the effect of the back reaction [42].

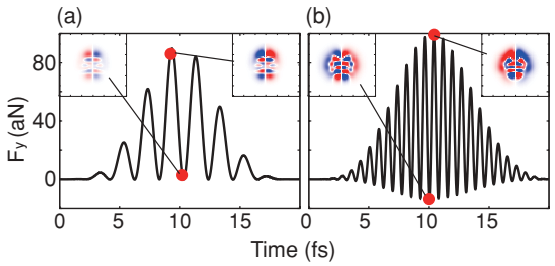

FIG. 2. (Color online) Time dependence of optical force on a silver particle exerted by the near field at (a) $\omega = 1.0$ eV (off-resonance) and (b) 2.7 eV (resonance). Insets are the snapshots of the induced electron densities where the red and blue show increases and decreases in the electron density, respectively, compared to those of the ground state.

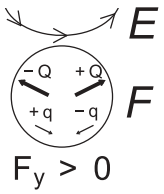

FIG. 3. Scheme for the optical force due to the interaction between inhomogeneously induced charges and a near field. The top curve with arrows shows the electric field, the sphere shows a nanoparticle, and Q and q are the polarization and screening charges, respectively. The black arrows indicate locally induced optical forces. The net optical force in the y direction is positive.

IV. RESULTS AND DISCUSSION

A. Silver nanoparticle

Figure 2 shows the time-dependent optical force exerted on the silver nanoparticle in the y direction calculated by Eq. (9) at (a) $\omega = 1.0$ eV (off-resonance) and (b) $\omega = 2.7$ eV (resonance) in units of attonewtons. Figure 2(a) clearly shows that the optical force is biased so that F_y takes a positive value during the excitation. This means that the near field induces an attractive force on the nanoparticle. On the other hand, under the resonance condition in Fig. 2(b), F_y takes both positive and negative values even though the force is also biased to the positive value. Focusing on the maximum values of F_y in these excitations, the resonantly induced optical force is slightly larger than the off-resonantly induced one. The time-averaged forces calculated by using Eq. (10) for each excitation are (a) 16.8 aN and (b) 16.9 aN. (As a reference, the gravitation acted on the nanoparticle is of the order of 10^{-15} aN.) This implies that the resonant condition does not necessarily significantly enhance the optical force.

The underlying mechanism of the near-field-induced optical force on the nanoparticle can be schematically explained. As shown in Fig. 1, in the near-field region, the electric field lines curve across the nanoparticle and the field intensity decreases with distance from the radiation source. When such a near field is applied to the nanoparticle, polarization charges ($\pm Q$) are induced in accordance with the curved electric field lines and the electron density distribution is biased; see the schematic of the induced charges in Fig. 3. In addition, the screening charges ($\mp q$) are generated as counterparts of the polarization charges ($\pm Q$). The terms of the polarization and screening charges were introduced to qualitatively explain the generation mechanism of the optical force. The computed results numerically take account of full contributions of these charges by solving the TDDFT calculations. Thus, the polarization and screening charges are not calculated separately, and we cannot clearly distinguish one from the other. Then, the local effective force is exerted on the polarization and screening charges, depending on both their distributions and their signs of the charge. A similar optical response is commonly found in conventional photoinduced phenomena, irrespective of whether a uniform or nonuniform electric field is applied to a nanoparticle. However, oscillating uniform electric fields, which have frequently been used in the studies of optical response under the dipole approximation, exert no net force on a time average because the uniform (or symmetric) polarization and screening charges are induced. On the other hand, since the near field is highly localized around a radiation source and the intensity of the field decreases rapidly with distance from the radiation source, net force is induced depending on the intensity gradient of the near field and on a balance between the amounts of the polarization and screening charges. In the present system, the force acting on the polarization charges (bold arrows in Fig. 3) is generally larger than on the screening charges (thin arrows). As a result, the near-field-induced optical force is biased so that the attractive force ($F_y > 0$) is exerted between the near-field fiber tip and the nanoparticle as shown in Fig. 2.

The actual electron dynamics is more complicated. The four insets in Fig. 2 illustrate the snapshots of time evolution of the polarization and screening charges on the x-y plane, where the red and blue indicate increases and decreases in the electron density, respectively, compared to those of the initial ground state. The charge distributions are complex but appear to be somewhat regular in the sense that those nodal patterns are antisymmetric to the y axis. Although it is difficult to clearly distinguish between the polarization and screening charges in the charge distribution, the snapshots of these charges are reminiscent of the schematic in Fig. 3. We computationally confirmed that in the resonance excitation [Fig. 2(b)] the polarization charges are induced in an inner region and the corresponding screening charges are localized around the nanoparticle surface. This is mainly because in the off-resonance excitation the electrons are forced to oscillate near the radiation source, whereas in the resonance excitation the specific electrons which are strongly associated with the details of the electronic structures primarily oscillate resonantly. Thus, in the resonance excitation, the optical force partly becomes negative because the net force is determined by a balance between the amounts of the polarization and screening charges.

Next, let us show the energy dependence of the optical force. Figure 4 shows the time-averaged force (red solid curve) and the absorption spectrum (black broken curve). The force spectrum was obtained by plotting the averaged optical force, varying the frequency by 0.1 eV from 0.8 to 3.6 eV. The absorption spectrum was obtained under a dipole approximation in a way similar to the previous methods [36,37]. The averaged force spectrum has peaks at 1.3 and 2.2 eV, which are different from the resonance

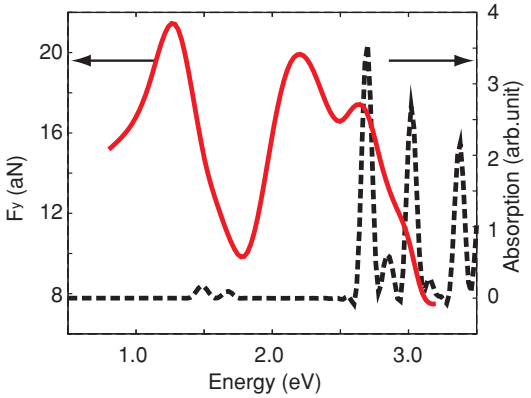

FIG. 4. (Color online) Absorption spectrum (dashed-black) of the silver nanoparticle and the time-averaged force on the particle (red) as a function of energy.

frequency. Although the polarization charges are significantly induced when the laser frequency is in tune with the resonance frequency, this figure proves that the resonance excitation does not necessarily maximally induce the net force. This is because the screening charges partly (and sometimes largely) cancel the polarization charges. As a result of the sensible balance between the polarization and the screening charges, several maxima and minima appear in the force spectrum. Conversely, this result indicates that we can manipulate atoms and molecules in nanostructures by controlling the strength of attractive force (and possibly repulsive force), changing the laser frequency. To do that, electronic structure calculations of target nanostructures must be carried out. Our electron dynamics approach combined with nonuniform light-matter interaction theory fulfills such a requirement.

Before discussing the results of C_{60}, we show the field-intensity dependence of the optical force. Since the present near field is approximated by the oscillating dipole in the form of Eq. (11), we calculated the intensity dependence by varying the dipole moment of the radiating source, which is associated with the field intensity. The laser frequency ω is set to 1.0 eV (off-resonance). Figure 5 shows the time-averaged optical force as a function of the square of the dipole moment of the radiation source. The x and y axes are shown in a

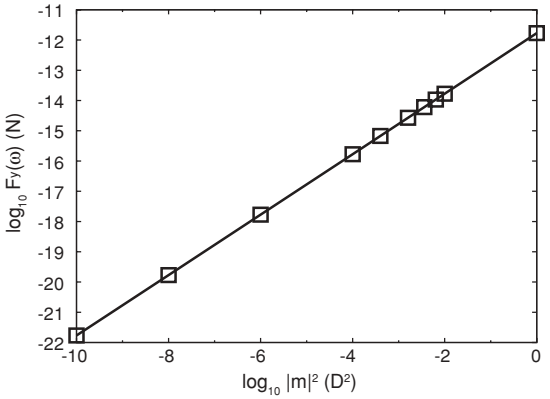

FIG. 5. Time-averaged force on the silver particle under the off-resonant condition (1.0 eV) as a function of the square of the dipole moment of the radiation source.

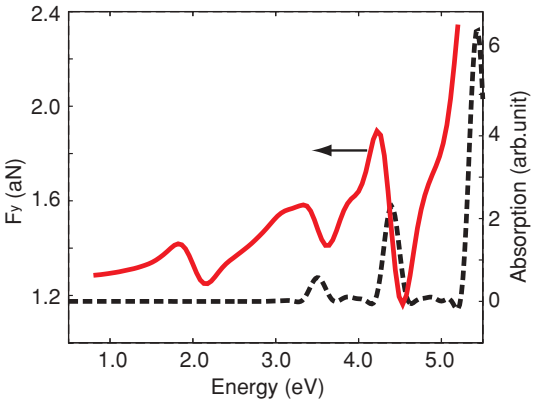

FIG. 6. (Color online) Same as Fig. 6 but for C_{60}.

logarithm scale with base 10. We found that the optical force is linearly proportional to the near-field intensity. The optical force amounts to 10^{-12} N when the radiation source has the moment of 1 D.

B. C_{60}

We have also calculated the optical force for C_{60} interacting with the near field. Contrary to the case of the metal particle, the force on C_{60} does not become negative both for off-resonant (1 eV) and resonant (3.6 eV) conditions. This can be attributed to the hollow structure of C_{60} because there are no effective screening charges. The time-averaged forces are 1.29 aN (off-resonance condition) and 1.41 aN (resonance condition). In this case, a stronger force is induced under the resonant condition than under the off-resonant condition. The force on C_{60} is an order of magnitude smaller than that on the silver particle because of lesser mobility of the charges and the absence of charges inside the sphere. We plot the time-averaged force (red solid curve) as a function of energy in Fig. 6. The absorption spectrum (black broken curve) is also drawn as a reference. The optical force has several peaks, similar to the force spectrum of the metal particle, and generally increases as a function of the energy. The figure clearly demonstrates that the optical force is largely determined by the detailed electronic structures of the molecule.

V. CONCLUDING REMARKS

We have calculated the near-field-induced optical forces acting on a silver particle mimicked by a jellium model and on C_{60}. The real-time and real-space TDDFT approach combined with the nonuniform light-matter interaction formalism, recently developed by the authors, was employed to accurately calculate the inhomogeneous charge polarization induced by the full multipole interaction with the near field. The induced force is reasonably explained in terms of the polarization and screening charges. The local optical force on the silver particle in the y direction takes both positive and negative values depending on the spatial distribution of these charges, and the net force becomes attractive as a result of a balance between the polarization and screening charges. The optical force on C_{60} is an order of magnitude smaller than that on the silver particle

because of the lesser mobility of the electrons. The energy dependence of the optical force of these particles showed several maxima and minima, indicating that the resonance excitation does not necessarily induce the optical force most efficiently. Such a nonmonotonic energy dependence of the optical force will be utilized when manipulating nanoparticles at the nanometer scale by controlling the near-field frequency. To calculate the optical forces induced by a highly nonuniform electric field in real molecules, a sensible balance of the polarization and screening charges must be determined. The present first-principles TDDFT approach, taking account of full light-matter interactions, can be a powerful tool for optical manipulation in nanostructures.

ACKNOWLEDGMENTS

The present work was supported by Grants-in-Aid No. 18066019 and No. 21350018 and by the Next-Generation Supercomputer Project from the Ministry of Education, Culture, Sports, Science and Technology of Japan. T.I. acknowledges financial support by the Japan Society for the Promotion of Science (No. 2003281).

[1] A. Ashkin, Phys. Rev. Lett. **24**, 156 (1970).
[2] A. Ashkin, J. M. Dziedzic, J. E. Bjorkholm, and S. Chu, Opt. Lett. **11**, 288 (1986).
[3] A. Ashkin, IEEE J. Sel. Top. Quantum Electron. **6**, 841 (2000).
[4] D. G. Grier, Nature (London) **424**, 810 (2003).
[5] K. C. Neuman and S. M. Block, Rev. Sci. Instrum. **75**, 2787 (2004).
[6] J. C. Crocker and D. G. Grier, Phys. Rev. Lett. **77**, 1897 (1996).
[7] B. Lin, J. Yu, and S. A. Rice, Colloids Surf. A **174**, 121 (2000).
[8] K. Svoboda and S. M. Block, Annu. Rev. Biophys. Biomol. Struct. **23**, 247 (1994).
[9] U. Seifert, Adv. Phys. **46**, 13 (1997).
[10] A. D. Mehta, M. Rief, J. A. Spudich, D. A. Smith, and R. M. Simmons, Science **283**, 1689 (1999).
[11] M. J. Lang and S. M. Block, Am. J. Phys. **71**, 201 (2003).
[12] L. Novotny and B. Hecht, *Principles of Nano-optics* (Cambridge University Press, New York, 2006).
[13] L. Novotny, R. X. Bian, and X. S. Xie, Phys. Rev. Lett. **79**, 645 (1997).
[14] K. Cho, Prog. Theor. Phys. Suppl. **106**, 225 (1991).
[15] J. K. Jenkins and S. Mukamel, J. Chem. Phys. **98**, 7046 (1993).
[16] O. Keller, Phys. Rep. **268**, 85 (1996).
[17] E. Lorin, S. Chelkowski, and A. Bandrauk, Comput. Phys. Commun. **177**, 908 (2007).
[18] K. Lopata and D. Neuhauser, J. Chem. Phys. **130**, 104707 (2009).
[19] K. Okamoto and S. Kawata, Phys. Rev. Lett. **83**, 4534 (1999).
[20] P. C. Chaumet and M. Nieto-Vesperinas, Phys. Rev. B **61**, 14119 (2000).
[21] A. I. Bishop, T. A. Nieminen, N. R. Heckenberg, and H. Rubinsztein-Dunlop, Phys. Rev. A **68**, 033802 (2003).
[22] T. Iida and H. Ishihara, Phys. Rev. Lett. **90**, 057403 (2003).
[23] V. Wong and M. A. Ratner, Phys. Rev. B **73**, 075416 (2006).
[24] T. Iwasa and K. Nobusada, Phys. Rev. A **80**, 043409 (2009).
[25] S. Mukamel, *Principles of Nonlinear Optical Spectroscopy*, Oxford Series on Optical and Imaging Sciences (Oxford University Press, New York, 1999).
[26] C. Cohen-Tannoudji, J. Dupont-Roc, and G. Grynberg, *Photons and Atoms: Introduction to Quantum Electrodynamics* (Wiley Interscience, New York, 1989).
[27] D. P. Craig and T. Thirunamachandran, *Molecular Quantum Electrodynamics* (Dover Publications, New York, 1998).
[28] E. Runge and E. K. U. Gross, Phys. Rev. Lett. **52**, 997 (1984).
[29] F. Calvayrac, P. G. Reinhard, E. Suraud, and C. A. Ullrich, Phys. Rep. **337**, 493 (2000).
[30] J. D. Jackson, *Classical Electrodynamics*, 3rd ed. (Wiley, New York, 1998).
[31] N. W. Ashcroft and N. D. Mermin, *Solid State Physics* (Brooks/Cole Thomson Learning, New York, 1976).
[32] N. Troullier and J. L. Martins, Phys. Rev. B **43**, 1993 (1991).
[33] L. Kleinman and D. M. Bylander, Phys. Rev. Lett. **48**, 1425 (1982).
[34] J. P. Perdew and A. Zunger, Phys. Rev. B **23**, 5048 (1981).
[35] J. R. Chelikowsky, N. Troullier, K. Wu, and Y. Saad, Phys. Rev. B **50**, 11355 (1994).
[36] K. Yabana and G. F. Bertsch, Phys. Rev. B **54**, 4484 (1996).
[37] K. Yabana and G. F. Bertsch, Int. J. Quantum Chem. **75**, 55 (1999).
[38] R. Baer and R. Gould, J. Chem. Phys. **114**, 3385 (2001).
[39] M. A. L. Marques, A. Castro, G. F. Bertsch, and A. Rubio, Comput. Phys. Commun. **151**, 60 (2003).
[40] K. Nobusada and K. Yabana, Phys. Rev. A **70**, 043411 (2004).
[41] K. Nobusada and K. Yabana, Phys. Rev. A **75**, 032518 (2007).
[42] J.-Y. Yan, W. Zhang, S. Duan, X.-G. Zhao, and A. O. Govorov, Phys. Rev. B **77**, 165301 (2008).